REPORT DOCUMENTATION PAGE

Form Approved
OMB No. 0704-0188

PLEASE DO NOT RETURN YOUR FORM TO THE ABOVE ORGANIZATION.

1. REPORT DATE *(DD-MM-YYYY)*	2. REPORT TYPE	3. DATES COVERED *(From - To)*
12-10-2011	Final Report	6/1/2008-5/31/2011

4. TITLE AND SUBTITLE
Quantification of Multiple Cracks Using MM-wave Antenna Sensor Network

5a. CONTRACT NUMBER
FA9550-08-1-0317

5b. GRANT NUMBER

5c. PROGRAM ELEMENT NUMBER

6. AUTHOR(S)
Haiying Huang

5d. PROJECT NUMBER

5e. TASK NUMBER

5f. WORK UNIT NUMBER

7. PERFORMING ORGANIZATION NAME(S) AND ADDRESS(ES)
University of Texas Arlington
500 W. First Street, Arlington, Texas 76019

8. PERFORMING ORGANIZATION REPORT NUMBER

9. SPONSORING/MONITORING AGENCY NAME(S) AND ADDRESS(ES)
Air Force Office of Scientific Research
Structural Mechanics Program

10. SPONSOR/MONITOR'S ACRONYM(S)
AFOSR

11. SPONSOR/MONITOR'S REPORT NUMBER(S)
AFRL-OSR-VA-TR-2012-0266

12. DISTRIBUTION/AVAILABILITY STATEMENT
A

13. SUPPLEMENTARY NOTES

14. ABSTRACT

In aerospace structures such as around the fastener holes, etc, multiple small cracks can emerge concurrently. These small cracks can elude inspections because of their small sizes. Sudden coalescence of these small cracks, however, could lead to a large crack in a short period of time, which may lead to catastrophic structural failures. The goal of this project is to develop a sensing mechanism that can track multiple crack growth with millimeter resolution. An innovative sensing concept of using a microstrip patch antenna for crack growth detection was investigated. The major achievements of the project are: 1) validated the effect of crack growth and crack orientation on the resonant frequencies of the microstrip antennas; 2) demonstrated wireless interrogation of the unpowered microstrip antenna sensors; 3) realized multi-sites crack detection using a four-antenna sensor array. Techniques to fabricate the microstrip antenna on flexible polyimide substrate as well as the associated interrogation circuit were developed. Numerical simulation of the antenna sensor was developed and validated with experiment results. Control software and data processing algorithm were developed to automate the wireless interrogation process. This project produced 7 published journal paper, 1 journal pap

15. SUBJECT TERMS

16. SECURITY CLASSIFICATION OF:			17. LIMITATION OF ABSTRACT	18. NUMBER OF PAGES	19a. NAME OF RESPONSIBLE PERSON
a. REPORT	b. ABSTRACT	c. THIS PAGE			Haiying Huang
					19b. TELEPHONE NUMBER *(Include area code)* 817-272-0563

Reset

Standard Form 298 (Rev. 8/98)
Prescribed by ANSI Std. Z39.18
Adobe Professional 7.0

Final Report for AFOSR Contract Number FA9550-08-1-0317
Quantification of Multiple Cracks Using MM-wave Antenna Sensing Network

Abstract: In aerospace structures such as around the fastener holes, etc, multiple small cracks can emerge concurrently. These small cracks can elude inspections because of their small sizes. Sudden coalescence of these small cracks, however, could lead to a large crack in a short period of time, which may lead to catastrophic structural failures. The goal of this project is to develop a sensing mechanism that can track multiple crack growth with millimeter resolution. An innovative sensing concept of using a microstrip patch antenna for crack growth detection was investigated. The major achievements of the project are: 1) validated the effect of crack growth and crack orientation on the resonant frequencies of the microstrip antennas; 2) demonstrated wireless interrogation of the unpowered microstrip antenna sensors; 3) realized multi-sites crack detection using a four-antenna sensor array. Techniques to fabricate the microstrip antenna on flexible polyimide substrate as well as the associated interrogation circuit were developed. Numerical simulation of the antenna sensor was developed and validated with experiment results. Control software and data processing algorithm were developed to automate the wireless interrogation process. This project produced 7 published journal paper, 1 journal paper under review, 10 conference presentations, and 2 patent applications. One master student graduated with the support of this project and 1 PhD student is expected to graduate in summer of 2011. Two undergraduate students participated in this project.

1. Introduction

Fatigue crack is a very common phenomenon in aging aircrafts. Even though more and more attention was paid during design, manufacturing, and maintenance phases to avoid fatigue failures, 50 to 90% of mechanical failures are due to fatigue development. An investigation report from the Major Airframe Fatigue Test (MAFT) on the Tornado fighter jet indicated that fatigue cracks around bolt holes, geometry (e.g. notches), cut outs (e.g. open holes), fasteners, and lugs etc. accounts for 70% of the total damages found. The bolt-holes were the second most common reason leading to an aircraft accident from 1947 to 1983, as reported by Campbell and Lahey. Statistics show that the number of aging aircraft (older than 15 years) was around 4730 in 1994. To maintain the airworthiness of these aging aircrafts, a rigorous inspection regime has to be carried out periodically. Despite of the aerospace industry's best practices, small fatigue cracks can still evade the inspections. Recent crack problem encountered by Southwestern Airline's fleet of Boeing 737s highlights the limitation of current inspection procedure. Among various types of fatigue cracks, Multi-Sites Damage (MSD) problem, defined as multiple small fatigue cracks initiate at different locations, is especially difficult to detect. Even though each individual crack may be shorter than the detectable crack size, the coalescence of these small cracks could produce a large continuous crack in a short period of time, causing sudden structural failures. Therefore, the capability to detect and monitor these small cracks at multiple locations is of paramount importance for safety assurance of aging aircrafts.

Many non-destructive crack detection techniques, such as visual inspection, dye penetration, radiography, eddy current, ultrasound, magnetic particle inspection, etc., have been developed in the past decades. Most of these techniques usually require disassembling the aircrafts so that the components can be tested in a lab setting. Therefore, frequent inspections of the structural

components can be cost-prohibitive and time-consuming. Even though visual inspection or non-destructive inspections using portable instruments do not require disassembling, these types of inspection are highly subjective and unreliable because they are operator-dependent. Structural Health Monitoring (SHM) could potentially address these shortcomings because the sensors are installed on the structures and the inspections can be performed autonomously. The most researched SHM technique is the piezoelectric wafer-based guided-wave crack detection schemes. By studying the interactions between a propagating guided-wave and the crack, crack detection over a large area using a few piezoelectric wafer actuators/sensors can be achieved. However, this method is not very sensitive to small cracks. Moreover, they are also susceptible to interferences from structure discontinuities that make extracting the crack information from the sensing signal difficult. Point sensors, i.e., sensors that detects crack near its vicinity, usually have much higher sensitivity than guided-wave based sensing schemes. One of such sensors is the Meandering Winding Magnetometer (MWM) sensor developed by JENTEK Sensors, Inc. In order to detect multiple cracks, however, several sensors have to be employed. Since each sensor requires an electric connection for signal transmission, the cable size becomes large as the number of sensors increases. Such a weight penalty is unaffordable on a weight-sensitive structure, such as for fighter jets. Another promising technique is the Comparative Vacuum Monitoring (CVM) sensors. The CVM sensor consists of a series of low vacuum and pressurized channels. A surface crack will create a passage between the low vacuum channels and the pressurized ones, causing a pressure change that provides an indication of crack presence. However, The CVM sensor cannot differentiate multiple cracks intersecting the longitudinal direction of the vacuum channels. In addition, a CVM–based system requires designated pressure sensors to measure each vacuum channel if high spatial resolution is required. This may be difficult to implement for multiple crack detection since multiple vacuum channels are needed.

Detecting small crack over a large area requires distributing multiple sensors at various locations. To simplify the sensor interface and the data collection process, sensor multiplexing is desired. Unfortunately, it is very difficult to implement sensor multiplexing for conventional sensors. One exception is the optical fiber sensors, which can be multiplexed based on various multiplexing mechanisms, including time-domain multiplexing (TDM), wavelength-domain multiplexing (WDM), frequency-domain multiplexing (FDM), combination of both TDM and WDM, and coherence multiplexing. This multiplexing capability makes optical fiber sensors the only feasible candidate for damage detection over a large area. However, optical fiber sensors are usually very fragile. Once damaged, an optical fiber cannot be repaired or reconnected. Besides, damaging the optical fiber at one location will disable all the downstream sensors.

This project investigates a new crack detection mechanism, i.e. using microstrip patch antenna for crack detection and monitoring. One unique advantage of the antenna sensors is that they can be remote interrogated without a local power source. Moreover, since the crack information is encoded in the resonant frequency of the antenna sensor, sensor multiplexing using frequency division is possible. Spatial division, i.e. installing the sensors at different location and activate the sensor one at a time, can also be implemented for sensor multiplexing. This report summarizes the achievements of these three-year project, including: 1) quantify the effects of crack on the radiation frequencies of antenna sensors; 2) demonstrate passive wireless interrogation technique; and 3) realize sensor multiplexing for multiple-crack detection and tracking.

2. Principle of Operation

2.1 Principle of Operation – Crack Detection

The crack detection sensor is based on a microstrip patch antenna that consists of a dielectric substrate with a ground plane on one side of the substrate and an antenna patch printed on the other side of the substrate (see figure 1a). The ground plane and the antenna patch, both conductive in nature, form an electromagnetic resonant cavity that radiates at distinct frequencies. The radiation characteristics of such antenna sensor can be represented by the S_{11} curves shown in figure 1(b). The resonant frequencies and return loss are the two important parameters describing the performance of an antenna sensor. The return loss indicates the radiation efficiency of the antenna whereas the resonant frequencies are the frequencies at which the return loss is a local minimum, as shown in figure 1(b). If the antenna patch is rectangular in

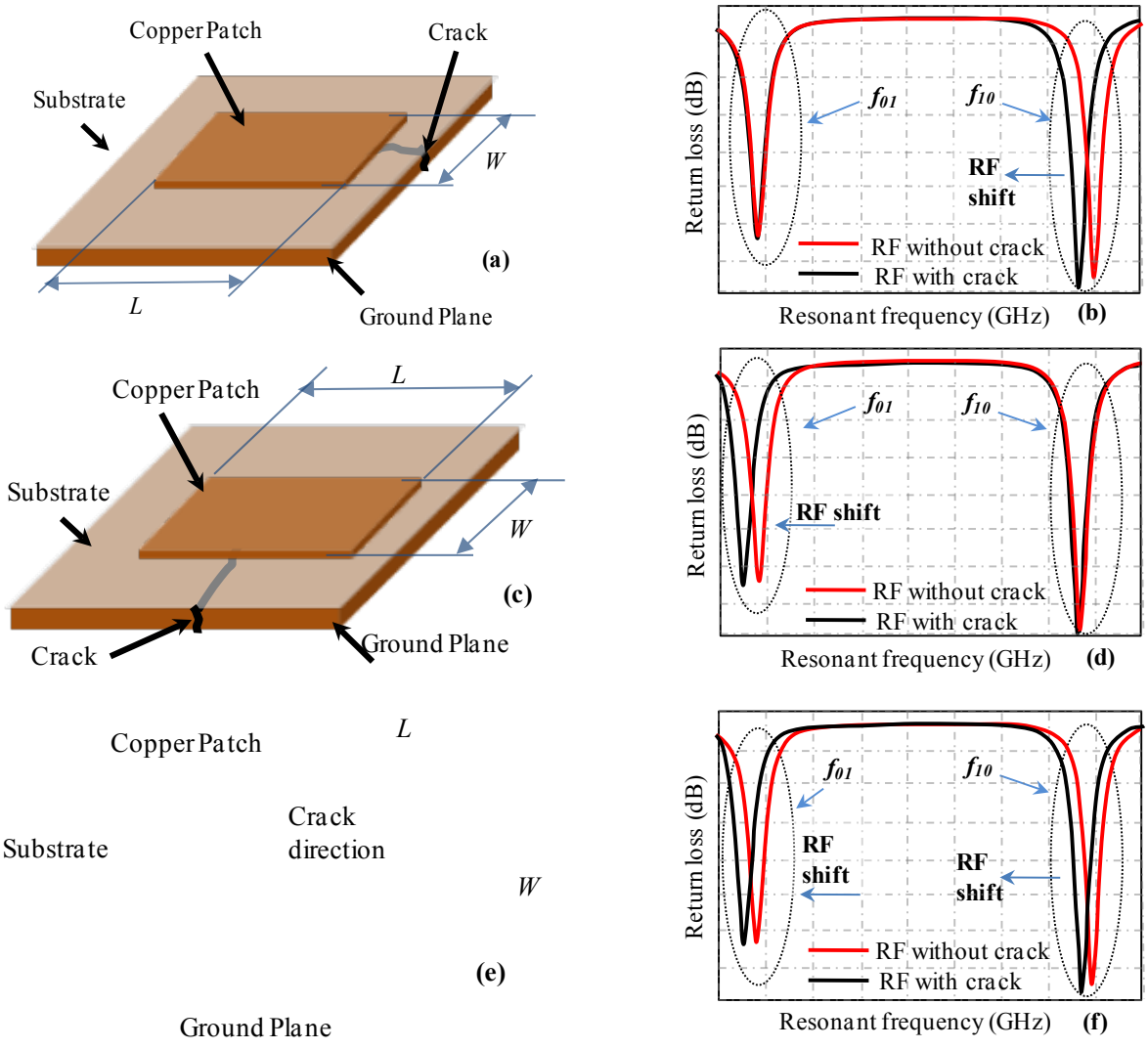

Figure 1: Principle of antenna sensor for crack detection; (a) & (b) antenna sensor with a crack along its length and its effect on the f_{10} frequency; (c) & (d) antenna sensor with a crack along its width and its effect on the f_{01} frequency; (e) & (f) antenna sensor with an inclined crack and its effect on both f_{10} and f_{01} frequencies.

shape, it radiates at two fundamental resonant modes; the TM_{10} mode whose electric field is parallel to the physical width of the antenna patch and the TM_{01} mode whose electric field is parallel to the physical length of the antenna patch. The resonant frequencies of these resonant modes are related to the corresponding electric field dimension as

$$f = \frac{c}{2\sqrt{\varepsilon_e}} \frac{1}{L_e + 2\Delta L_c}, \quad (1)$$

where c is the velocity of light in vacuum, ε_e is the effective dielectric constant of the substrate, and ΔL_c is the line extension. L_e is the electric length of the radiation mode, which is the geometrical dimension of the antenna patch that is parallel to the respective electric current direction, assuming the ground plane is perfectly conductive. Therefore, a rectangular antenna patch having a larger dimension along its length direction will have a lower TM_{01} resonant frequency f_{01} and a higher TM_{10} resonant frequency f_{10}. The conductivity of the ground plane also influences the resonant frequencies. When a crack is introduced along the length direction of the antenna patch, it partially cuts off the current flow along the width direction and forces the current to flow around the crack. As a result, the current path along the width direction is increased, essentially increasing the electrical length of the TM_{10} mode. Since the resonant frequency is inversely proportional to the electrical length, the resonant frequency f_{10} reduces with the crack growth (see figure 1b). The amount of reduction in the f_{10} frequency is determined by the overlapping length between the crack and the antenna patch, i.e., the crack length underneath the antenna patch. On the other hand, the TM_{01} current flow is not disturbed by the crack since the crack is parallel to its current flow. Therefore, the resonant frequency f_{01} remains the same as if there is no crack presence. A crack that is parallel to the width direction of the patch will have exactly the opposite effect on the f_{01} and f_{10} frequencies as compared to a crack that is parallel to the length direction of the antenna patch, as shown in figure 1(c) and 1(d). If an inclined crack is introduced, the current flows along both the directions of the patch are distorted (see figure 1e). This distortion increases the electrical lengths of both radiation modes. As a result, both resonant frequencies will shift towards lower frequencies (see figure 1f). Since each different crack orientation changes the resonant frequencies of the antenna sensor in a different way, the crack orientations can be identified from the resonant frequency shifts of the antenna sensor.

2.2 Principle of Operation – Unpowered Wireless Interrogation

One unique advantage of the antenna sensor is that it can be wirelessly interrogated based on the principle of antenna backscattering. When a wideband interrogation signal is broadcasted to an antenna sensor, the signals whose frequency matches with the resonant frequency of the antenna sensor will be received by the antenna sensor. If the antenna sensor is not terminated with a perfectly-matched load, the received signal will be reflected at the antenna termination and re-radiated by the antenna sensor. This re-radiated signal is called the antenna mode backscattering, which has the same frequency as the resonant frequency of the antenna sensor. As a result, the resonant frequency of the antenna sensor can be determined from the spectrum of the antenna mode backscattering. However, the structural

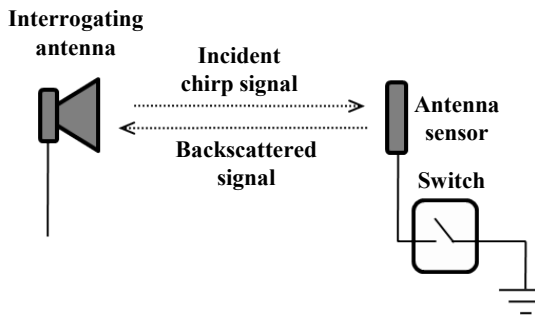

Figure 2: Wireless interrogation based on impedance switching and backscattering.

mode backscattering, i.e. the signals reflected by the surrounding structures, is in general several orders higher in power than the antenna mode backscattering. In order to isolate the antenna mode from the structural mode, an impedance-switching mechanism is needed. As shown in figure 2, the antenna sensor is terminated with a switch, which can switch the antenna termination from short-to-ground to open. Since the antenna mode backscattering has a 180 degree phase shift between these two states while the structural mode backscattering remains the same, the structural mode backscattering can be canceled by subtracting the backscattered signals at these two termination states. In our case, a light-activated microwave switch was implemented. As a result, the antenna sensor can be wirelessly interrogated by illuminating the microwave switch using a light beam.

2.3 Principle of Operation – Sensor Multiplexing

The wireless antenna sensor can be multiplexed based on the principles of frequency division and spatial division. The frequency division of a dual-antenna sensor array is shown in figure 3. As shown in figure 3(a), the two antenna sensors are designed to have different patch lengths so that they radiate at different f_{01} frequencies. Before the crack reaches one of the antenna sensor, the frequency spectrum of the signal backscattered by the dual-antenna sensor array, i.e. the blue curve in figure 3(b), displays two resonant peaks; the lower frequency f_{01l} is the f_{01} frequency of

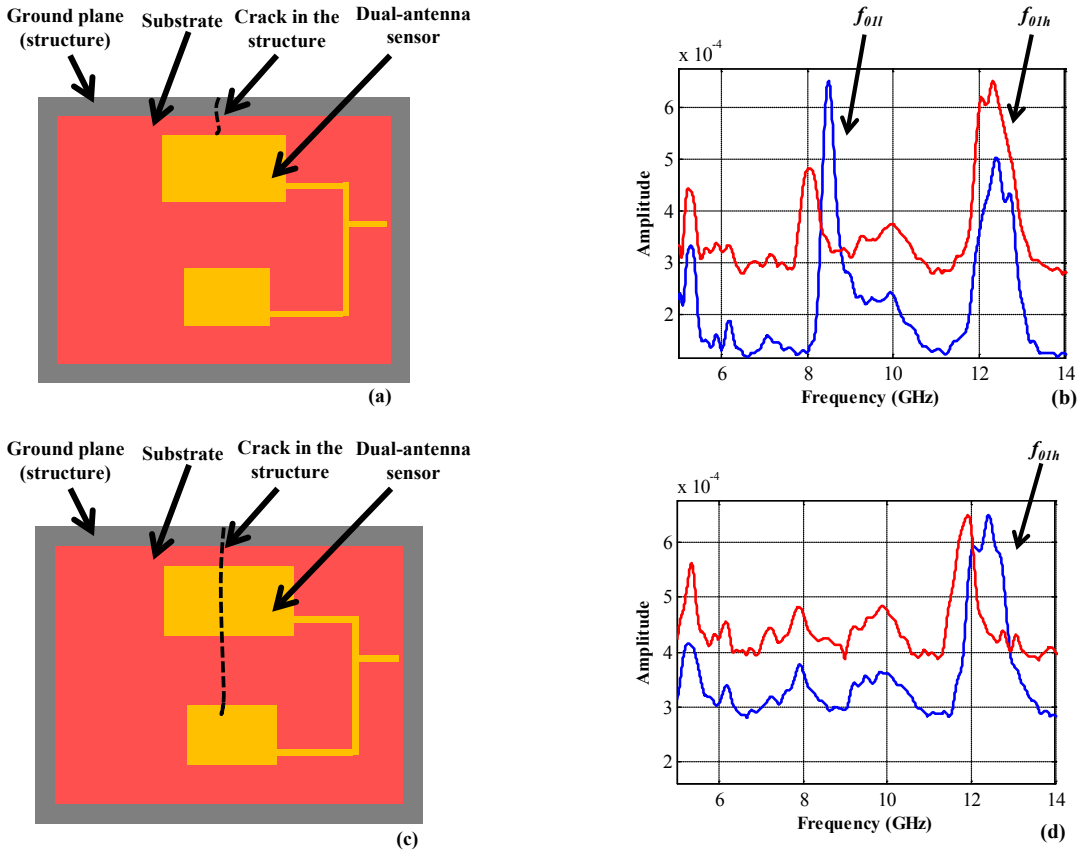

Figure 3: Frequency division of a dual-antenna sensor array: (a) a short crack underneath the large antenna; (b) effect of short crack on spectrum of normalized antenna signal; (c) a long crack underneath the small antenna; (d) effect of long crack on spectrum of normalized antenna signal.

the large antenna sensor while the higher frequency f_{01h} corresponds to the f_{01} frequency of the small antenna sensor. Assume a crack that is perpendicular to the length direction of the antenna patch is present underneath the large antenna sensor, the f_{01l} resonant frequency shifts to a lower value while the resonant frequency f_{01h} remains the same, as indicated by the red curve in figure 3(b). Similarly, a crack propagating underneath the small antenna sensor reduces the f_{01h} frequency while has no influence on the f_{01l} frequency (see figure 3c and 3d). The amounts of decrease in these frequencies are directly correlated to the crack length underneath the antenna patch. Therefore, the propagation length of the crack can be tracked by monitoring the successive shift of the antenna resonant frequencies. The f_{10} resonant frequencies of both antenna sensors remain the same since the width-direction crack does not disturb the current flow along the width direction.

The spatial division of two dual-antenna sensor arrays is shown in figure 4. The two dual-antenna sensor arrays have identical radiation characteristics but are installed at different locations. Each antenna sensor array is equipped with its own impedance-switching circuit. When the interrogation of the first antenna sensor array is called for, the light switches its impedance switching circuit on and off to obtain the backscattered signals at two termination states. The illumination light for the second antenna sensor array remains the same for both states. Therefore, the signal backscattered by the second antenna sensor array is counted as the structural backscattering and thus does not contribute to the normalized backscattered signal. Subsequently, the second antenna sensor array can be activated by switching its illumination light while keeping the first antenna sensor array inactive. This spatial division scheme enables the individual interrogation of multiple antenna sensor arrays sequentially, even if they share the same resonant frequencies. We investigated the combination of these two multiplexing schemes to achieve simultaneous interrogation of a single dual-antenna sensor array and sequential interrogation of multiple antenna sensor arrays to achieve sensor coverage over a large area.

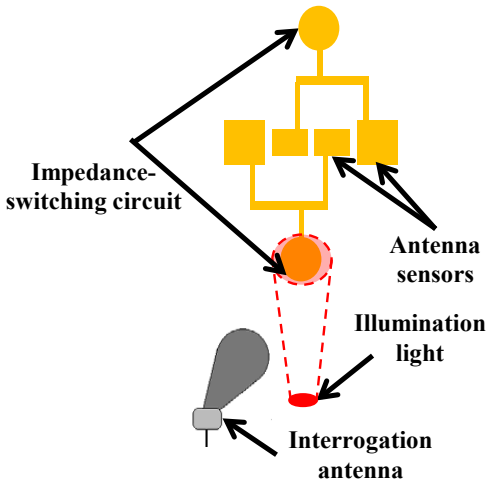

Figure 4: Selective interrogation of multiple dual-antenna sensors based on spatial division.

3. Research Tasks and Procedure

3.1 Develop Techniques for Wireless Interrogation of unpowered Antenna Sensor

In order to interrogate the antenna sensor wirelessly, a light-activated switching circuit was implemented using a Pseudomorphic High Electron Mobility Transistor (pHEMT, ATF36077 from Avago Technologies) and a photocell (Clare model – CPC 1832). The integration of the antenna sensor and the light-activated switching circuit is shown in figure 5. The patch antenna was fabricated by bonding a dielectric substrate (Kapton HN, 125 μm in thickness, dielectric constant ε_r = 3.4) on a compact tensile specimen using fatigue-certified glue, followed by bonding the antenna patch on the dielectric substrate using super glue. The antenna patch pattern

and the transmission line were cut from a copper tape (3M 118, 68 μm in thickness, 12.75 mm in width, and 15 mm in length) using a sharp blade. The source terminal of the pHEMT, the anode of the photocell, and the ground of the 560 KΩ resistor were bonded to the antenna ground plane using conductive epoxy. The inset-fed antenna sensor was connected to the drain terminal of the pHEMT through a microstrip transmission line. The gate terminal of the pHEMT was connected to the cathode of the photocell. The pHEMT offers an open circuit from its drain terminal to the ground plane when its gate voltage is kept at -0.8 V and a short circuit when its gate voltage is 0 V. The 580 KΩ resistor was employed to reduce the voltage output (at constant-current) of the photocell from an open circuit value of 8 V to 0.8 V when it was exposed to a light beam generated by a flash light. To make sure that the photocell produces a stable output, the light beam should be strong enough so that the photocell is operating in saturation. It was observed that the ambient light was not sufficient to cause any change in the pHEMT biasing.

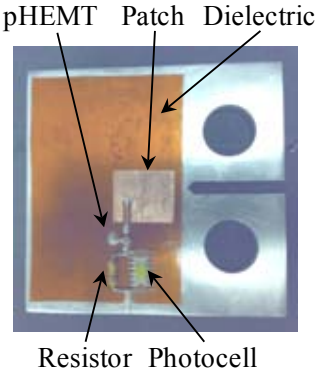

Figure 5: passive antenna sensor with a light-activated RF switch.

The experiment set up for characterize the wireless interrogation of the antenna sensor is shown in figure 6. The interrogation horn antenna is placed at a distance of 1.34 m from the antenna sensor. A Microsoft Excel program was developed to control the light source and the VNA, which initiates the VNA at the beginning of the test, triggers the VNA to collect data at different antenna termination states, receives the data and stores them in the hard drive of the computer. Each measurement consists of two steps. The spectrum of the backscattered signal was first measured when the light source was turned OFF. At this state, the pHEMT is in saturation mode and the antenna sensor is shorted to the ground. The light source was then turned ON to bias the

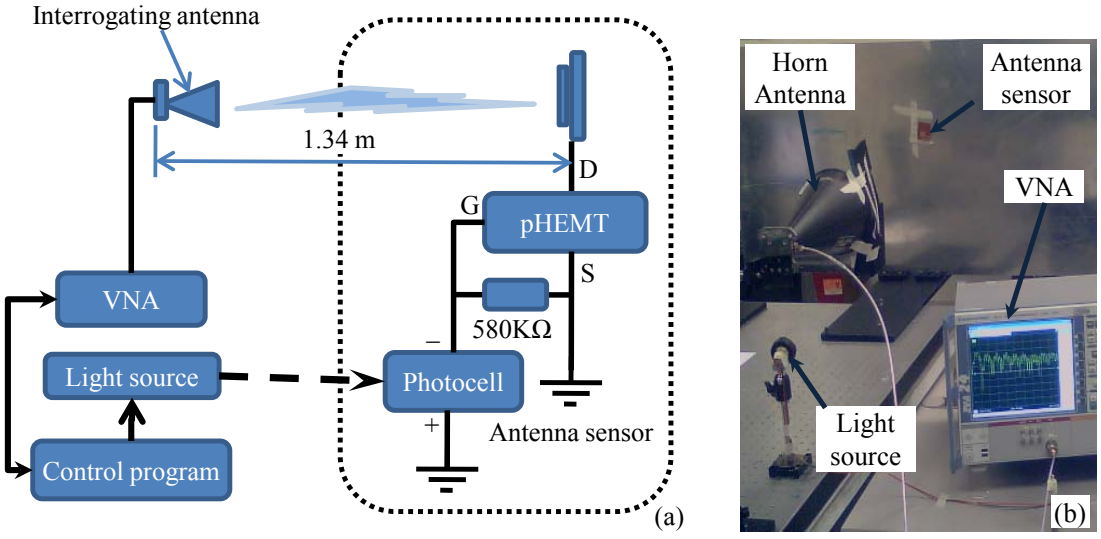

Figure 6: Wireless interrogation of passive antenna sensor: (a) diagram; (b) experimental implementation.

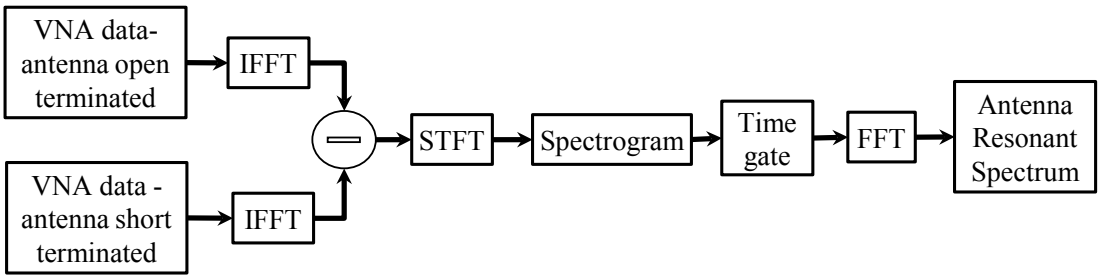

Figure 7: Signal processing of measurement data.

pHEMT into the cut-off mode and thus terminate the antenna sensor in open circuit. The VNA was again triggered to collect the spectrum of the backscattered signal. These two sets of data should be subtracted to isolate the antenna mode backscattering from the structural mode backscattering. In addition, the VNA measures the frequency components of the backscattered signal over a long time span. The arrival of the antenna mode backscattering, on the other hand, is determined by the distance between the interrogating antenna and the antenna sensor. Therefore, the signal-to-noise ratio (SNR) of the antenna mode signal can be improved by time gating the normalized backscattered signal. In order to perform time gating, the frequency domain signal measured by the VNA must be converted to time domain first. After time gating, the time domain antenna mode signal again needs to be converted back to frequency domain to extract the resonant frequency of the antenna sensor. A digital signal processing program, therefore, is needed to perform the time gating, the frequency-time domain conversions, and the normalization scheme. A flow diagram of the signal processing algorithm is shown in figure 7. The two measurement data files are imported into the program first. Subsequently, the frequency-domain signals are converted to time-domain signals using Inverse Fast Fourier Transformation (IFFT). The time-domain signals are then subtracted to obtain a normalized signal that supposedly contains the antenna mode backscattering only. Next, a short-time Fourier Transformation (STFT) is performed to display the time-frequency components of the normalized signal, based on which the starting and ending time of the antenna mode backscattering can be selected. Finally, the normalized antenna mode signal is time gated and is converted to frequency domain using Fast Fourier Transformation (FFT). Based on the frequency spectrum of the time gated antenna mode backscattering, the resonant frequency of the antenna sensor corresponding to the polarization of the interrogating signal can be determined.

The frequency of the backscattered signal depends on the polarization orientation of the interrogating horn antenna. If the polarization of the horn antenna is parallel to the width dimension of the antenna sensor, the center frequency of the backscattered signal should be the same as the f_{10} frequency of the antenna sensor. If the antenna sensor is rotated by 90 degrees, the center frequency of the backscattered signal should be the f_{01} frequency of the antenna sensor since the polarization of the horn antenna is aligned with the length direction of the antenna sensor. To characterize the effect of the antenna orientation on the frequency of the backscattered signal, an experimental set-up allowing the antenna sensor to be precisely rotated about three directions, i.e. the elevation, azimuth, and polarization direction, was implemented (see figure 8). The polarization axis of the antenna sensor was parallel to the axis of the horn antenna, the elevation axis was parallel to the antenna length direction, and the azimuth axis was parallel to the antenna width direction. The antenna sensor was placed at a distance of 53 inches from the

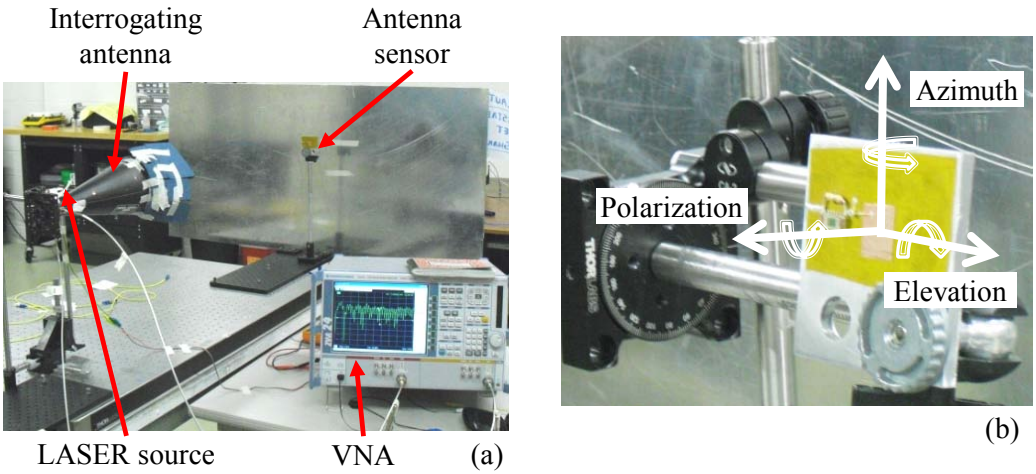

Figure 8: Experiment setup for angular response measurement of the antenna sensor: (a) actual setup; (b) rotation directions.

interrogating horn antenna. A laser pointer was placed next to the horn antenna, pointing at the photocell on the antenna sensor. By connecting the horizontal feed of the horn antenna to the VNA, the polarization of the horn antenna radiation was aligned along the elevation axis, i.e. the length direction, of the antenna patch. The antenna resonant frequencies were measured at an elevation angle of -45, -30, -10, 0, and 10 degrees, an azimuth angle of -45, -30, 0, 10, 30, and 45 degrees, and a polarization angle of 0, 10, 30, 45, 60, and 90 degrees.

3.2 Investigate the effect of crack on antenna resonant frequency

Experiment procedure and simulation models were developed to understand the effect of the crack on the resonant frequencies of the antenna sensors. The effects of crack growth as well as crack kinking are quantified.

Effect of Crack Growth on the Resonant Frequency of Antenna Sensors – Fatigue Testing

Remote interrogation of the antenna sensor during fatigue testing is shown in figure 9. The CT specimen was mounted on a mechanical testing frame using clevises and pins. A CCD camera was placed facing the opposite side of the antenna sensor. Digital images of the cracked region of the specimen were acquired using a LabView program into a computer and displayed on a monitor to track the crack propagation. The horn antenna, placed in front of the antenna sensor at a distance of 36 inches, was connected to port 1 of a Vector Network Analyzer (VNA), which was configured to sweep from 5 GHz to 9 GHz in 8000 points. The VNA was calibrated with its reference plane at the end of the cable and the power output of the VNA was set to 25 dBm. A light source was used to illuminate the photocell and thus activate the impedance switching. The brightness of the light source was adjusted to maintain a -1.5 volt gate-to-source voltage for the

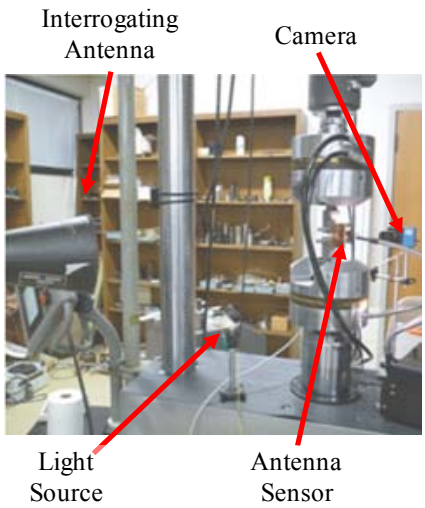

Figure 9: Fatigue test of wireless antenna sensor.

pHEMT. The light source was triggered using the computer's parallel port through a relay (OEG model OUAZ-SS-105D). Whenever the crack reached a reference mark, the fatigue cycling was paused at a static load of 300 lbs. The resonant frequency of the antenna sensor was then measured by triggering a measurement sequence using the Microsoft Excel program. The measured spectra were downloaded from the VNA to a computer for data processing. Ten measurements were recorded for each crack length and the average resonant frequency was calculated. After completing the measurement process, the fatigue cycling was resumed until the crack reached the next reference mark. The fatigue test was continued until cracking of the antenna patch was observed due to large crack opening.

Effect of Crack Direction on the Resonant Frequency of Antenna Sensor

To study the effect of crack direction on the resonant frequency of the antenna sensors, the antenna sensors were fabricated on a laminate board so that the crack can be machined in the ground plane using a milling machine. This arrangement facilitates precise control of the crack orientation as well as rapid parametric study. The laminate board (Rogers 4350B) has a dielectric constant of $\varepsilon = 3.66$ and has 35 µm thick copper films on both sides. After cutting the laminate board into 2 inch long and 1.5 inch wide rectangular pieces, the antenna patch was milled on one side of a laminate board using a mini-milling machine, Turbo carver. The outline of the antenna patch was first formed on the laminate with a fine cutter (0.1 mm thick), followed by machining off the copper surrounding the antenna patch with a wider cutter. The copper on the other side of the laminate, which forms the ground plane of the antenna sensor, was left intact. After masking the antenna patch and the ground plane with a strain gage tape, the board was dipped in Ferric Chloride solution for ten to fifteen minutes to etch off the remaining copper around the antenna patch. Once the copper was completely etched, the laminate was rinsed thoroughly in water and dried. The masking tape was then removed and the antenna sensor was thoroughly cleaned with acetone to remove any residual taping. To connect an SMA connector to the antenna sensor, the antenna sensor was sandwiched between an aluminum block and a plastic plate. The SMA connector was then mounted on the aluminum block with its pin touching the end of the antenna sensor feed line. The antenna sensor can then be connected to a Vector Network Analyzer through the SMA connector to measure the S_{11} parameter of the antenna sensor. Thin slots (0.7 mm width) were machined in the ground plane of the antenna sensor to imitate the cracks. The experimental setup to machine the crack using a milling machine is shown in figure 10(a). The milling machine was custom-made by mounting a high speed pneumatic carver (Turbo carver TC550, see figure 10b) on a SuperScribe™ Circuit Board Prototyping System from Micro Kinetics Corporation. The vertical depth of the cutting tool was precisely controlled to be 35 µm, which corresponds to the thickness of the ground plane. The SMA/sensor assembly was placed underneath the cutting tool with its antenna patch facing down so that cracks can be milled in the ground plane of the antenna sensor. The crack was initiated at one of the edges of the antenna patch. Whenever the crack reached a reference

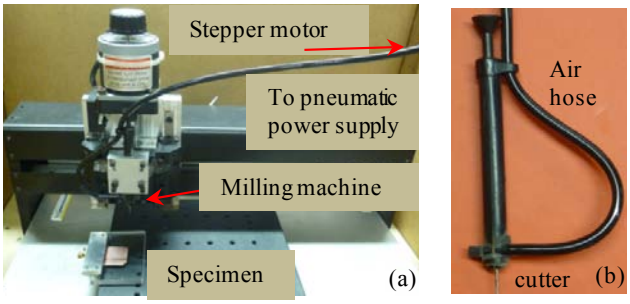

Figure 10: Experimental setup for crack propagation; (a) SuperScribe™ circuit board prototyping system; (b) high speed pneumatic carver.

mark, the antenna sensor assembly was removed from the milling machine and the S_{11} parameter of the antenna sensor was measured on a VNA. The measurement was done at each reference mark until the crack passes through the entire length of the antenna patch.

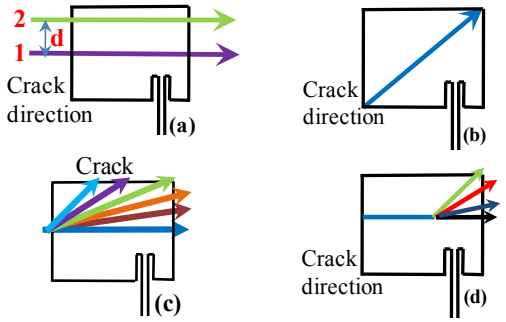

Figure 11: Crack configurations; (a) crack parallel to the length and at a distance *d* from center line; (b) crack along the diagonal of the patch; (c) cracks at various inclination angles; (d) kinked cracks.

The antenna design was simulated using a commercial program HFSS™. The substrate was assumed to have a relative permittivity of 3.66 and a relative permeability of 1. The antenna patch and the ground plane are assumed to be made of perfect electric conductors; the patch and the ground plane were 35 μm thick. The antenna patch was excited at the end of the microstrip line with a 50-ohm lumped port. The size of the spatial cells in HFSS discretization was roughly $\lambda_d/10$, where λ_d is the wavelength corresponding to the dielectric substrate's material. The simulation model was validated by comparing the simulated results with the measurements. The effect of four crack configurations, as shown in figure 11, on the antenna resonant frequencies was investigated using the experiment and simulation methods.

3.3 Realizing sensor multiplexing for multiple-crack detection and tracking

Since the location of the crack is not known a priori, a sensor array is needed to cover a large area in order to detect small cracks. In this project, we investigated multiplexing the antenna sensors to form a sensor array using both frequency division and spatial division. For frequency division, a two-antenna array with each antenna operating at different frequency is needed. We designed two single antenna sensors first. The dimensions of the two antenna sensors are 10.4 by 8.6 mm and 7.2 by 6 mm respectively, as shown in figure 12. A substrate dielectric constant of 2.5 results in the f_{01} resonant frequencies of 8.4 GHz and 12 GHz for the two antenna sensors. The 3.6 GHz frequency spacing between these two resonant frequencies ensures that the higher

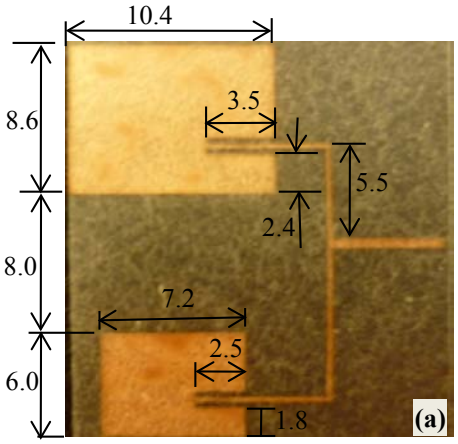

Figure 12: Antenna design; (a) dimensions of dual-antenna sensor array; (b) four-antenna sensor array.

resonant frequency will not overlap with the lower resonant frequency even if there is a through crack under the 6 mm antenna patch. When the feeding structure as shown in figure 12(a) is used to connect the two antenna sensors, the coupling between the two antenna sensors has to be considered which is influenced by the spacing between the two antenna sensors, the dielectric constant of the substrate, and the width of the antenna sensor. In our case, the distance between the two antennas was chosen to be 8 mm. At this separation distance, the coupling between the two single antenna sensors is negligible. Since the two antennas share one impedance-switching circuit, a 100 Ω main feed line was designed to connect the two 50 Ω feed lines. The S_{11} parameters of the antenna array with different main feeding positions were simulated using an EM simulation tool, Sonnet Pro. The simulations indicated that the return losses of the two antennas are about -25 dB and -22 dB when the main feed line is located at 5.5 mm away from the feed line of the large antenna. Based on our past experience, this return loss is low enough for the remote interrogation of the antenna sensors. When the two antenna arrays are placed in close proximity, the presence of one antenna array may influence the gain of the other antenna array. According to the technology of parasitic metallic bar, the gain of a patch antenna can be enhanced if it is surrounded by a metallic strip. For our sensor arrangement, the antenna sensor array that is not activated can serve as the parasitic metallic bar for the small antenna of the activated antenna array if the non-activated antenna sensor array is disconnected from the ground during the interrogation process.

A fatigue specimen with edge cracks emanating from two circular holes was designed in order to validate the antenna sensor array's capability to detect cracks at multiple locations, as shown in figure 13(a). This specimen imitates a section of fuselage with a row of fastener holes. Sufficient space was designed between the two pre-cracked holes to allow installing the two dual-antenna sensor arrays for crack detection and monitoring between the holes. The width of the MSD specimen was designed to be 101.6 mm. According to the ASTM standard E647-00, a clevis with multiple bolts is required for gripping such a wide specimen. The bolt holes were designed to have a diameter of 12.7 mm and a hole spacing of 35.6 mm. The gage length, i.e. the distance between the two rows of the bolt holes was chosen to be 182.7 mm. The enlarged view of the machined crack is shown as the insert in figure 13(a). The machined slots, imitating a crack originating at one edge of the hole, are 12.7 mm in length. After machining the specimen out of a

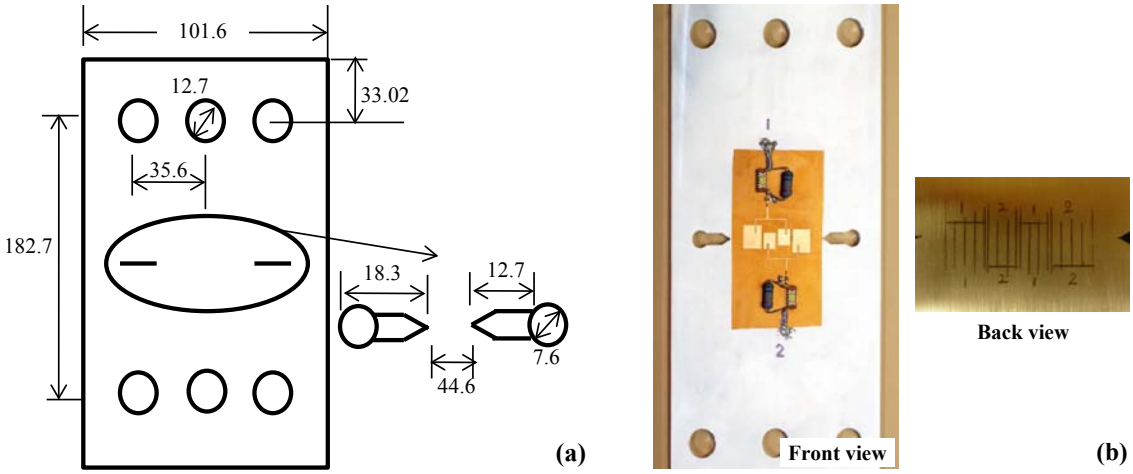

Figure 13: MSD fatigue specimen: (a) specimen dimensions; (b) specimen with sensors installed.

7075-T6 Aluminum alloy plate using a CNC machine, a 300 μm diameter diamond wire was used to cut a 1 mm long slot on either side of the machined slots to produce sharp crack tips. The machined MSD specimen was first sanded using 220, 400, 600, and 1500 grit sand papers to obtain a flat and smooth surface. At the position where the dielectric substrate (Kapton FN, 76 μm in thickness, 80 mm in length, and 42 mm in width) is supposed to be bonded, a 600 grit sand paper was used to roughen the surface to ensure a good bonding between the substrate and specimen. The antenna sensors were laser machined (Oxford Lasers E-355-3 OA System) and bonded on top of the dielectric substrate. Light-activated microwave switches were mounted on the MSD specimen following the same procedure as those described above. The specimen instrumented with the antenna sensor array is shown in figure 13(b). The two dual-antenna sensors were placed symmetrically at the center so that we can compare their performance. The positions of the antenna sensors as well as 2 mm spaced reference marks were drawn on the opposite side of the MSD specimen so that the crack growth can be visually monitored during fatigue test using a digital camera, as shown in figure 13(b).

4. Research Results and Discussions

4.1 Wireless interrogation of the antenna sensor

The spectra of the antenna mode backscattering for various elevation angles are shown in figure 14(a). The SNR was the highest when the antenna sensor was oriented at zero degrees. As the angle of rotation increased, the resonance peak remained at the same frequency while the SNR reduced. This indicates that the measured antenna frequencies are not very sensitive to the angular alignment. The f_{10} frequency of the antenna sensor can be reliably measured as long as the antenna sensor and the horn antenna were aligned within 30 degrees. The spectra of the antenna mode backscattering at different azimuth angles are shown in figure 14(b). Again the frequency peak locations were not sensitive to the angle changes but the SNR is. The maximum SNR was achieved at an azimuth angle of 30 degrees instead of zero degree. This might be contributed by the feed line not locating along the center line of the patch, which could produce a radiation pattern that is not symmetric about the zero degree azimuth angle. Rotating the antenna sensor along the polarization direction essentially changes the orientation of the antenna patch relative to the polarization of the horn antenna radiation. At zero degree, the width direction of the antenna patch was parallel to the polarization of the horn antenna radiation. Therefore, only the f_{10} frequency was observed (see figure 14c). For a polarization angle increase up to 45 degrees, the f_{10} frequency behaved similarly as when the elevation and azimuth angle was increased, i.e. the resonance frequency remained at the same frequency while the SNR decreased. At a polarization angle of 60 degrees, the f_{01} frequency started to emerge and the f_{10} frequency disappeared. At 90 degrees, the length direction of the antenna patch was aligned with the polarization of the electromagnetic field. As such, only the f_{01} frequency was visible. Even though the f_{10} frequency was insensitive to the polarization angles up to 45 degrees, the f_{01} frequency seems to be more sensitive to the polarization angle arrangement, e.g. at 60 degree polarization angle, the f_{01} frequency peak was not as distinguishable as the f_{10} frequency peak at 30 degree polarization angle. This might be explained by the radiation patterns. Due to the feed line configuration, the radiation patterns of these two radiation modes are different. Nevertheless, this experiment demonstrated that the two fundamental resonant frequencies of the antenna sensor can be remotely interrogated using one rotating horn antenna or using a horn antenna with dual polarizations.

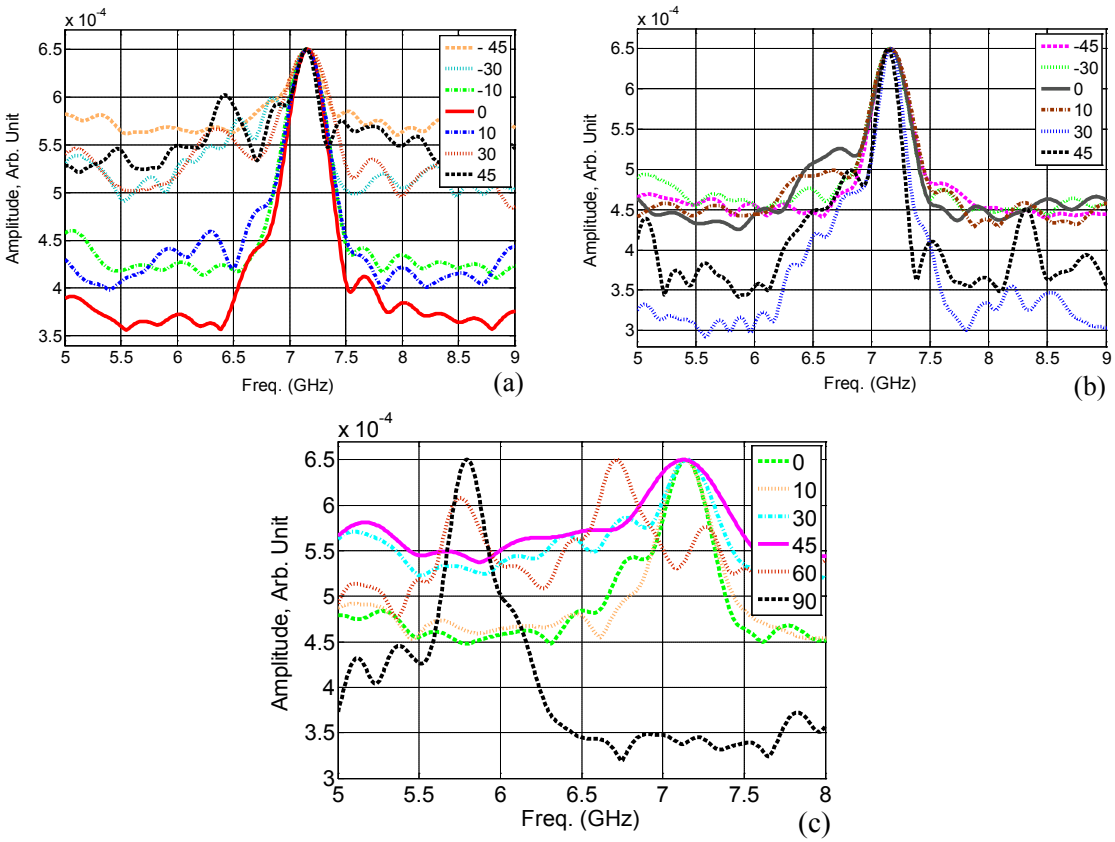

Figure 14: Angular response of the antenna sensor: (a) elevation direction; (b) azimuth direction; and (c) polarization direction.

4.2 Effect of Crack Growth on Antenna Resonant Frequency – Single Antenna

The shift of the antenna frequency with the crack growth, acquired from the fatigue test of a signal antenna sensor, is shown in figure 15. The rightmost curve (blue color) in figure 15(a) represents the f_{10} frequency of the antenna sensor when the crack was at the left edge of the antenna patch, *i.e.* there was no overlap between the crack and the antenna patch. Each subsequent shift of the curve to the left corresponds to a crack propagation of 1 mm. The signal strength of the backscattered antenna mode signal reduced with the crack growth. As a result, the Signal to Noise Ratio (SNR), defined as the ratio between the amplitude of the antenna mode and the average amplitude of the noise floor, also reduced. Cracking of the antenna patch right above the crack was observed as the crack opening increased with the crack growth. This might have contributed to the reduction of SNR. Defining the left edge of the antenna patch as the origin of the crack tip location and normalizing the frequencies at different crack lengths with the antenna frequency at crack location 0, the shift of the f_{10} frequencies obtained using three different methods, *i.e.* wireless interrogation, numerical simulation, and wired measurement, are compared in figure 15(b). It worth noting that the simulation model was simplified to reduce computation time, *e.g.* the thickness of the ground plane was assumed to be zero. A full scare three-dimensional simulation of the antenna sensor may result in better agreements but the required computation time is prohibiting. Even though the relationship between the frequency shift and the crack growth is not linear, the crack length can be determined from the frequency shift as

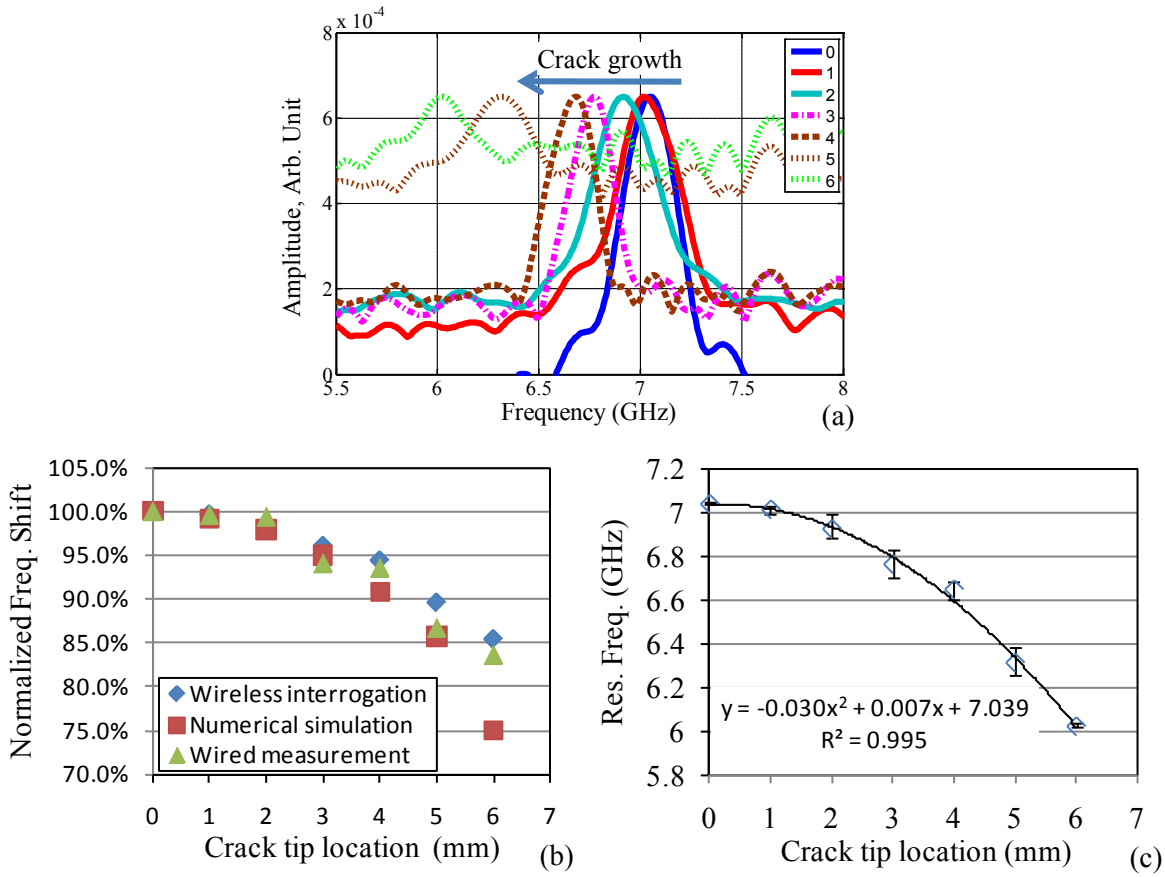

Figure 15: Effect of crack on the f_{10} frequency of the antenna sensor under a 300 lbs load: (a) shift of the antenna mode spectrum with crack growth; (b) comparison of normalized f_{10} frequency shifts obtained by wireless interrogation, numerical simulation, and wired measurements; (c) shift of the f_{10} frequency with crack growth (the average and error bar at location 1mm and 6mm were calculated from 4 and 5 measurements, respectively. The other data points were calculated from 10 measurements).

long as the relationship is calibrated. As shown in figure 15(c), the shift of the wirelessly measured f_{10} frequencies with the crack length fit a second order polynomial very well. From location 0 to location 1, 1 mm of crack growth shifted the f_{10} frequency by 24.85 MHz. As the crack grew under the antenna patch, the crack sensitivity increased steadily. From location 5 to location 6, 1 mm of crack growth resulted in a frequency shift of 292.5 MHz. Judging from the error bars presented in figure 15(c), we are confident that sub-millimeter crack growth can be detected using the antenna sensor.

4.2 Effect of Crack Growth on Antenna Resonant Frequency –Antenna Array

The effect of crack growth on the resonant frequencies of the four-antenna array is shown in figure 16. The measured data obtained from two dual-antenna sensors matched very well. For the large antenna sensor, the total frequency reduction was around 1% when the overlapping crack length was less than 3 mm. It worth noting that the antenna sensors are operating in the gigahertz frequency, a 1% frequency shift, therefore, is equivalent to tens of megahertz in absolute frequency shift. Therefore, we can conclude that a sub-millimeter crack length can be easily detected using the antenna sensors. At an overlapping crack length of 4 mm, the antenna

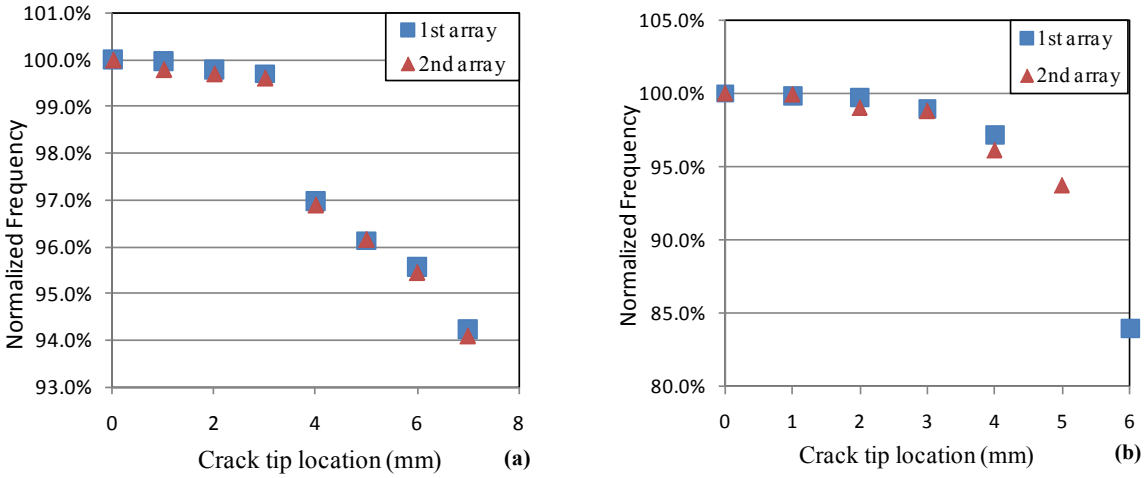

Figure 16: Comparison of normalized f_{10} frequencies obtained from two dual-antenna sensor arrays; (a) large antenna sensor; (b) small antenna sensor.

frequency was about 97% of its original value. When the overlapping crack length was more than 4 mm, the frequency shift was linearly proportional to the crack growth. The crack detection sensitivity is 1% in frequency shift for every 1 mm of crack growth. We were able to interrogate the large antenna until the crack reached the last 1 mm of its patch width. Once the crack tip reached the small antenna sensor, its growth can be monitored from the frequency shift of the small antenna. Therefore, we only have a "blind spot" of 2 mm in which the crack growth was not monitored. The resonant frequency of the small antenna sensor behaved similar to that of the large antenna sensor but it is more sensitive than the large antenna sensor. When the overlapping crack length was smaller than 3 mm, the frequency shifted 0.5% for every 1 mm of crack growth. The crack sensitivity increased to 2.5% per 1 mm of crack growth once the overlapping crack length was more than 3 mm. These results match very well with those obtained from the single antenna sensor. When the two cracks linked up to form a continuous crack, we were able to interrogate the small antenna in the first antenna array but not the one in the second antenna array. The total frequency reduction for the small antenna in the first antenna array was 16%.

4.3 Effect of Crack Orientation on Resonant Frequency of Antenna Sensors

To investigate the effect of crack orientation on the resonant frequencies of the antenna sensors, the first configuration we studied was a crack parallel to the length direction of the antenna patch and at a distance d from the horizontal center line (see figure 17a). This configuration is chosen to be the same as those we tested in the fatigue experiments so that the experiment results obtained from this study can be compared with those from previous study. Two cracks were studied for this crack configuration. Crack "1" passes through the center of the antenna patch while crack "2" is offset from the center by a distance d = 5 mm. The shift of the measured S_{11} curves with the growth of crack "1" is shown in figure 17(b). The right most curve (the blue curve) represents an overlapping crack length of 0 mm, i.e., the crack has just reached the left edge of the antenna patch. The leftmost curve (the black curve) was obtained when the crack has propagated through the entire patch. Each sequential S_{11} curve in between these two curves represents a crack propagation of 4 mm. Similar to what we have observed in fatigue

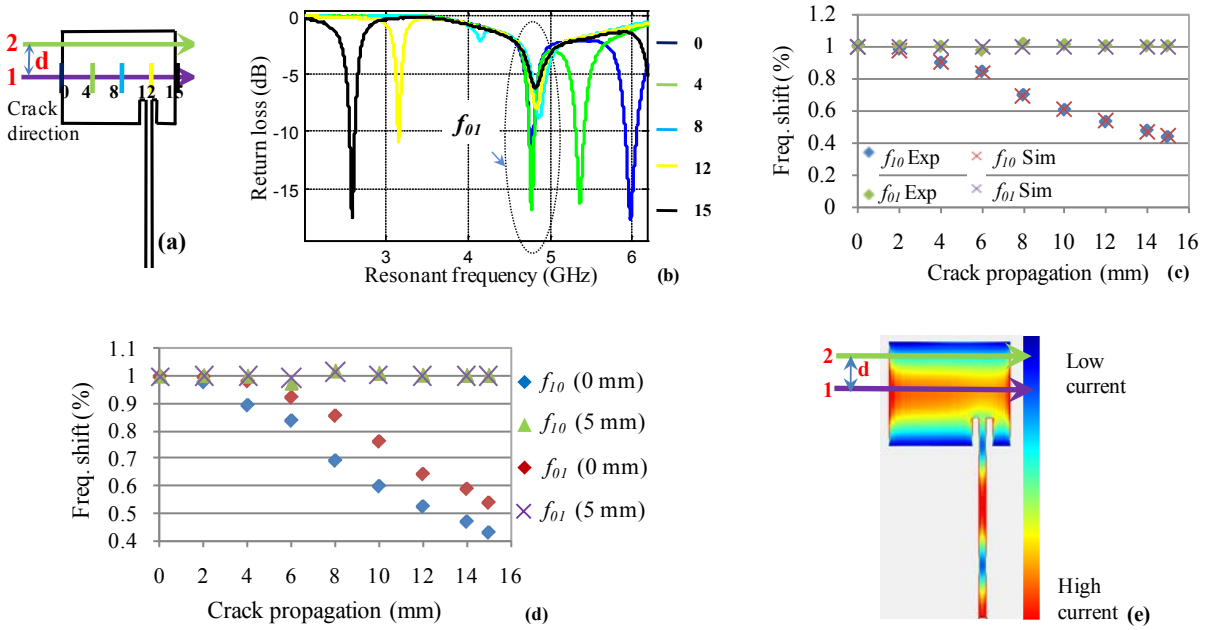

Figure 17: Effect of a crack passing perpendicular to the width at an offset to the center of the patch; (a) crack configuration; (b) shift of S_{11} curves with crack growth; (c) experimental and simulated f_{10} and f_{01} frequencies at different crack tip locations; (d) effect of crack offset on the resonant frequency shift; (e) current distribution along TM_{10} radiation mode.

experiments, the f_{10} resonant frequency shifted towards the lower frequency while the f_{01} resonant frequency remained almost constant. The measured f_{10} and f_{01} frequencies of the antenna sensor at various crack tip positions are compared with the simulated results in figure 17(c), which matched well with the simulation results for both resonant frequencies. Figure 17(d) compares the f_{10} and f_{01} frequency shifts of the antenna sensor containing crack "2" with those of the sensor containing crack "1". We observe that the slope of the frequency shift is the same for both cases, implying the antenna sensor can detect both cracks with similar sensitivity. However, crack "2" will not be detected until it is 2 mm past the left edge of the antenna patch. This phenomenon can be explained by studying the current distribution pattern of the TM_{10} radiation mode. As shown in figure 17(e), the current density along the TM_{10} mode is much higher at the center of the patch and gradually reduces toward the edges of the antenna patch. The crack propagating along the center line disturbs the high current density region. As a result, it causes a frequency shift as soon as it is underneath the antenna patch. On the contrary, a crack that is at a distance from the center line of the antenna patch passes through the low current density region. Therefore, a longer crack length is required to cause an observable frequency shift. An antenna sensor with a smaller width dimension may help reducing this blind zone, as evidenced by the data obtained from the antenna array experiment. The f_{01} resonant frequency remained constant in either case because the current along the length direction was not disturbed.

In order to evaluate the capability of the antenna sensor to detect the crack orientation, a crack was introduced along the diagonal of the antenna patch (see figure 18(a)). Both the f_{10} and f_{01} frequencies of the antenna sensor, once again obtained from the S_{11} curves, are plotted against the crack tip locations in figure 18(b) and 18(c). The total length of the diagonal crack

underneath the patch is around 19.87 mm (diagonal length for a patch 15.25 mm long and 12.75 mm wide). As expected, both the resonant frequencies shifted towards the lower frequency as the crack propagated under the antenna patch. The f_{10} resonant frequency, as shown in figure 18(b), has two dwell regions and one high sensitivity region. This phenomenon can be explained with the current distribution of the TM_{10} radiation mode shown in figure 18(d). Whenever a crack is propagated diagonally, it initially propagates through the low current density region at the corner, which results in a lower frequency shift. This justifies the first dwell region. After 4 mm of crack propagation in the low current density region, the crack enters the high current density region. As a result, the f_{10} resonant frequency starts to shift towards the lower frequency. The crack propagation also changes the current distribution of the TM_{10} mode. At a crack length of 8 mm, the high current region is "pushed" to the left side of diagonal crack. When the crack reaches 12 mm, the current is confined in the left-top corner of the antenna patch. As a result, further increase in crack propagation does not affect the current density distribution much. This explains the second dwell region in the f_{10} resonant frequency shift. On the other hand, the f_{01} resonant frequency has one dwell region only. To gain a better insight on the f_{01} resonant frequency, the TM_{01} radiation mode was studied. Figure 18(e) represents the current distribution along the TM_{01} radiation mode of the antenna sensor. It can be observed that the current density is higher along the horizontal edges, around the inset feed and at the center of the patch antenna. The resonant frequency of the antenna sensor is almost constant for the first 6 mm of crack propagation due to the low current density region at the corner of the patch. As the crack propagates beyond 6 mm, it enters the high TM_{01} current density region thereby causing the f_{01} frequency to shift towards the lower frequency. As the crack propagates, the high current density region is shifted along with the crack. This explains why the f_{01} resonant frequency continues to shift towards the lower frequency even after the crack propagates beyond the original high current density region.

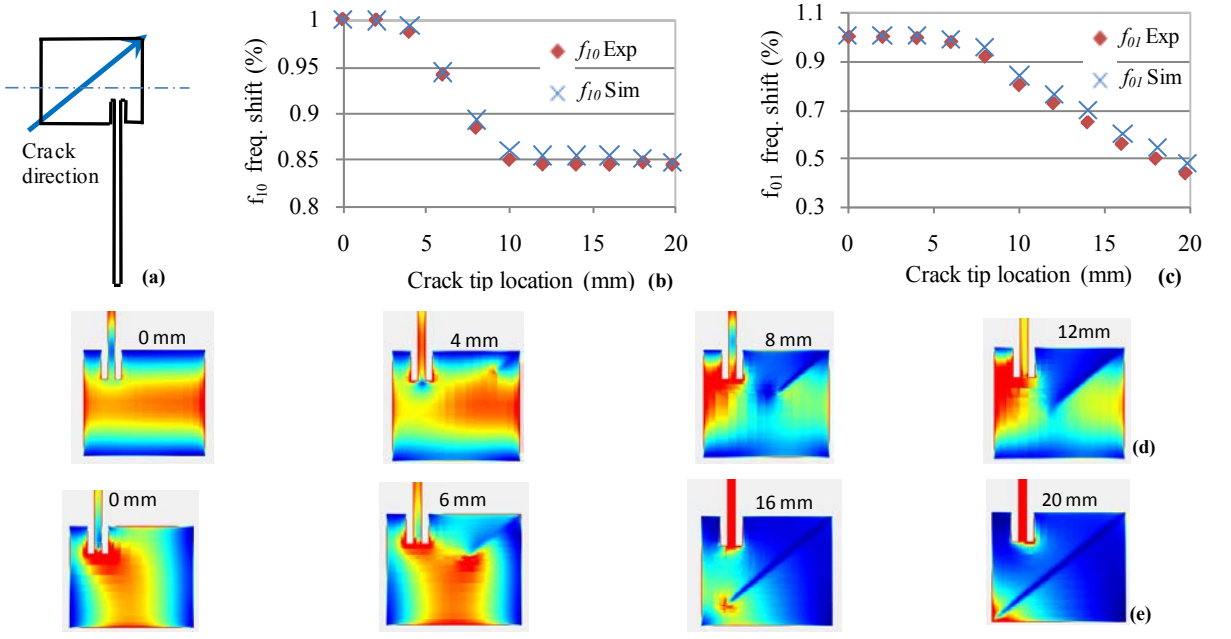

Figure 18: Effect of diagonal crack on the antenna sensor: (a) crack configuration; (b) f_{10} resonant frequency shift vs. crack tip locations; (c) f_{01} resonant frequency shift vs. crack tip locations; (d) TM_{10} mode current distribution with a diagonal crack; (e) TM_{01} mode current distribution with a diagonal crack.

The effect of a crack on the structural integrity depends on the relative inclination angle between the loading direction and the crack propagation. It is therefore very important for a sensor to detect the inclination angle of a crack. To evaluate the effect of inclined cracks on the resonant frequencies of the antenna sensor, the crack was initiated at the center of the antenna's left edge and then propagated at five different inclination angles (15, 20, 30, 45 and 60 degrees)(see figure 19(a)). Similar to the previous experiments, both the f_{10} and f_{01} frequencies of the antenna sensor were obtained from the S_{11} curves. However, analyzing two different frequencies (f_{10} and f_{01}) separately to evaluate the crack position and orientation angle was tedious. To simplify the data processing, a single parameter R is introduced to represent the effect of the crack on the two resonant frequencies. R is defined as the ratio between the normalized f_{01} and f_{10} frequencies, where the normalized resonant frequencies at a given crack length were calculated by dividing them with their counterparts at zero overlapping crack length. Figure 19(b) shows the frequency ratio R at various crack tip locations. For small inclination angles, the frequency ratio increases with the crack propagation. This is due to the fact that the f_{10} frequency reduces with the crack propagation while the f_{01} frequency remains almost constant. For the large angles, the frequency ratio reduces with the crack propagation since the f_{10} frequency shift is higher than the f_{01} frequency shift. Each inclination angle corresponds to a unique frequency ratio trend. Therefore, by tracking the change of the frequency ratio R, the crack propagation and orientation can be determined. Figure 19(b) also includes the effect of a diagonal crack, i.e. the 1st crack configuration, on the frequency ratio. As the diagonal crack has an inclination angle of 40 degrees to the length direction of the patch, the frequency ratio trend looks similar to that of a 45 degree inclined crack. The total crack propagation for the diagonal crack is much longer since it was initiated at the left-lower corner of the antenna patch.

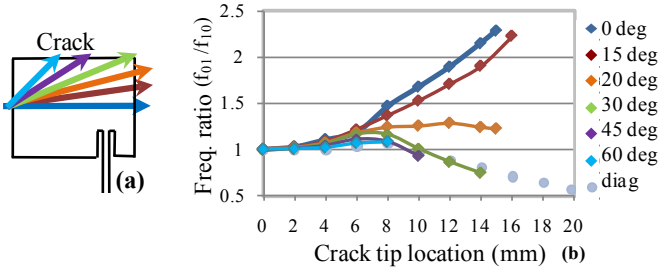

Figure 19: Effect of various inclination angles on antenna frequency; (a) schematic of crack propagation; (b) frequency ratio vs. crack tip locations.

In realistic scenarios, a crack may initially propagate along one direction and then change its propagation direction. These kinked cracks could be very dangerous because it might change the crack propagation pattern completely. In order to evaluate the effect of a kinked crack on the antenna sensor, a straight crack propagating along the length direction centerline was introduced first. The orientation of the crack was then changed to propagating along different angles (10, 30, 40 degrees) after it reached the center of the antenna patch (see figure 20a). Again, both the frequencies were

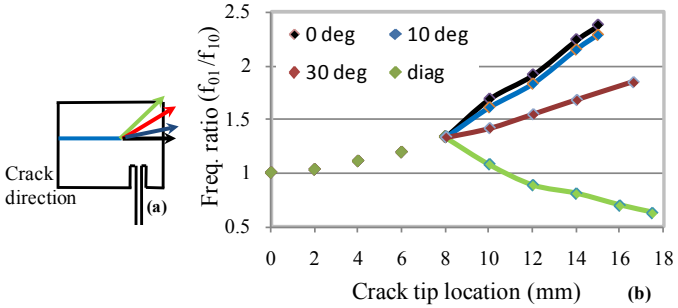

Figure 20: Effect of crack kinking on the antenna frequency; (a) schematic of crack propagation; (b) frequency ratio vs. crack tip locations.

obtained from the S_{11} curves and the frequency ratio R at various crack tip locations was plotted in figure 20(b). Since the crack was parallel to the length of the antenna patch for the first 8 mm, the trend of the normalized frequency ratio is similar initially. Once the crack changes its orientation, the frequency ratio changed accordingly. This is probably because the first 8 mm of straight crack growth has changed the radiation current density. Nonetheless, figure 20 (b) clearly indicates that crack kinking can be detected and measured from the frequency ratio R.

5. Conclusions

This project demonstrated sub-millimeter crack growth detection at multiple locations using unpowered wireless antenna sensor arrays. Wireless interrogation of the unpowered antenna sensor array was realized through the invention of a light-activated impedance-switching circuit and the associated data processing algorithm. Experiment procedures and numerical simulation model were established to characterize the effect of crack growth and crack orientation on the microstrip antenna sensor. Sensor multiplexing using frequency division and spatial division was achieved.

Appendix: Archival Publications During Reporting Period

Peered-reviewed Journal Publications:

1. Mohammad, I., Gowda, V., Zhai, H. and **H. Huang**, "Detecting crack orientation using Patch antenna sensors", accepted, *Measurement Science and Technology*
2. Deshmukh, S., Xu, X., Mohammad, I. and **Huang, H.**, 2011, "Antenna sensor skin for fatigue crack detection and monitoring", *Smart Materials and Systems,* Special Issue on Bio-inspired Sensing and Actuation, v8, n1, p93-106.
3. Mohammad, I. and **Huang, H.**, 2011, "An antenna sensor for crack detection and monitoring", *Advances in Structural Engineering*, 14, p47-53.
4. Mohammad, I. and **Huang, H.**, 2010, "Monitoring fatigue crack growth and opening using antenna sensors", *Smart Materials and Structures*, 19, p055023.
5. Deshmukh, S. and **Huang, H.**, 2010, "Wireless interrogation of passive antenna sensor", *Measurement Science and Technology*, v21, p035201.
6. Tata, U., Deshmukh, S., Chiao, J.C., Carter, R., and **Huang, H.,** 2009, "Bio-inspired sensor skins for structural health monitoring", *Smart Materials and Structures*, Special issue, v18, p104026. (Cited: 2)
7. Tata, U., **Huang H.**, Chiao, J.C., and Carter, R., 2009, "Exploiting patch antenna for strain measurement", *Measurement Science and Technology*, v20, p015201.

Conference Proceedings:

1. Mohammad, I. and **Huang, H.**, "Improving the reliability of sensor skins for fatigue crack monitoring", 9th International Workshop on Structural Health Monitoring, Stanford University, Sept. 2011.
2. Xu, X. and **Huang, H.**, "Multiplexing wireless antenna sensors for crack growth monitoring", SPIE-Smart Structures and Materials and NDE for Health Monitoring and Diagnostics, San Diego, CA, March 2011.
3. Mohammad, I. and **Huang, H.**, "Detecting crack orientation using antenna sensor", SPIE-Smart Structures and Materials and NDE for Health Monitoring and Diagnostics, San Diego, CA, March 2011.

4. Xu, X., Deshmukh, S., Mohammad, I. and **Huang, H.**, "Passive wireless sensor skin for crack detection and monitoring", *invited paper*, 5th World Conference on Structural Control and Monitoring, Shinjuku, Tokyo, July 2010.
5. Deshmukh, S., Mohammad, I., Xu, X., and **Huang, H.**, "Unpowered antenna sensor for crack detection and measurement", SPIE-Smart Structures and Materials and NDE for Health Monitoring and Diagnostics, San Diego, CA, March 2010.
6. Deshmukh, S., Mohammad, I., Wu, T., Tentzeris, M., and **Huang, H.**, "Crack detection and monitoring using passive wireless antenna sensor", ASME Conference on Smart Materials, Adaptive Structures and Intelligent Systems, SMASIS2009, California, 2009.
7. Mohammad, I., and **Huang, H.**, "Passive wireless patch antenna sensor for crack detection", 8th International Workshop on Structural Health Monitoring, Stanford University, Sept. 2009.
8. Mohammad, I. and **Huang, H.**, "An antenna sensor for crack detection and monitoring", ANCRISST workshop, Boston, 2009.
9. Tata, U., **Huang, H.**, Debb, S., Wang, J., and Chiao, J.-C., "A patch antenna-based strain sensor for structural health monitoring", SPIE Micro/MEMS, 2008.
10. Tata, U., **Huang H.**, Chiao, J.C., and Carter, R., "Bio-inspired sensor skins for structural health monitoring", ASME Conference on Smart Materials, Adaptive Structures and Intelligent Systems, SMASIS2008, Ellicott City, Maryland , Oct. 28-30, 2008.